

# Numerical Determination of Transmembrane Voltage Induced on Irregularly Shaped Cells

G. PUCIHAR, T. KOTNIK, B. VALIČ, and D. MIKLAVČIČ

Faculty of Electrical Engineering, University of Ljubljana, Ljubljana, Slovenia

(Received 03 May 2005; accepted 23 December 2005; published online: 18 March 2006)

**Abstract**—The paper presents an approach that reduces several difficulties related to the determination of induced transmembrane voltage (ITV) on irregularly shaped cells. We first describe a method for constructing realistic models of irregularly shaped cells based on microscopic imaging. This provides a possibility to determine the ITV on the same cells on which an experiment is carried out, and can be of considerable importance in understanding and interpretation of the data. We also show how the finite-thickness, nonzero-conductivity membrane can be replaced by a boundary condition in which a specific surface conductivity is assigned to the interface between the cell interior (the cytoplasm) and the exterior. We verify the results obtained using this method by a comparison with the analytical solution for an isolated spherical cell and a tilted oblate spheroidal cell, obtaining a very good agreement in both cases. In addition, we compare the ITV computed for a model of two irregularly shaped CHO cells with the ITV measured on the same two cells by means of a potentiometric fluorescent dye, and also with the ITV computed for a simplified model of these two cells.

**Key words**—Finite elements modeling, Induced transmembrane voltage, Di-8-ANEPPS, Electroporation, Electroporabilization.

## INTRODUCTION

When a biological cell is exposed to an external electric field, the induced transmembrane voltage (ITV) forms on its membrane.<sup>17,18,35</sup> The amplitude of the ITV is proportional to the amplitude of the applied electric field, and with a sufficiently strong field, this leads to a strong increase in membrane permeability. As a result, molecules for which the membrane is otherwise impermeable can be transported across the membrane. With appropriate duration and amplitude of the field, the phenomenon (termed electroporation or electroporabilization) is reversible and holds great potential for application in biochemistry, molecular biology, and many fields of medicine.<sup>31,43</sup> It has already become an established method in oncology (electrochemotherapy

of tumors)<sup>16,27,29,36</sup> and holds great promises in gene therapy.<sup>11,37,40</sup>

Increased permeability is localized to the regions of the cell membrane where the ITV exceeds a certain critical threshold, which is in the range of 200–1000 mV, depending on the cell type.<sup>42,44</sup> In order to obtain an efficient cell permeabilization it is therefore important to determine the distribution of the ITV on the cell membrane. The ITV varies with the position on the cell membrane, is proportional to the electric field, and is influenced by cell geometry and physiological characteristics of the medium surrounding the cell.<sup>7,21,26,33,35</sup> For an isolated cell of a simple shape, such as a cylinder, a sphere, or an ellipsoid, the ITV can be described analytically.<sup>9,10,21–23,35</sup> If the cell geometry is more complicated, or when cells are close enough to affect the electric field around each other, an analytical description is in general not attainable, and the ITV can be determined either experimentally (e.g. with potentiometric fluorescence dyes)<sup>2,13,15,20,25,30</sup> or numerically (e.g. using finite elements modeling<sup>5,6,28,32,39,45</sup> or resistive-capacitive [RC] transport lattices).<sup>12,38</sup>

In tissues, both complicated geometry and dense cell distribution are commonly the case. The experimental approach, which is simple and efficient with suspended cells or with cells growing in monolayers, is of limited use in tissues, where only the surface and a thin layer beneath it are directly accessible to standard microscopy techniques. For determination of the ITV on cells in tissues, the numerical methods are thus often the only feasible approach. The main problems of these methods are related to realistic modeling of a cell and—perhaps even more importantly—of its membrane. First, the models in which the cell is built with simple geometric shape or by combining several simple geometric shapes are usually only rough approximations of the actual cell shape.<sup>3,5,6,45</sup> Second, as the cell membrane is over a thousandfold thinner than the dimensions of a typical cell, even in models that use an adaptive mesh size, the thickness of the cell membrane is usually exaggerated by at least an order of magnitude.<sup>19</sup> This can be compensated partly by assigning to the membrane a higher specific conductivity,

Address correspondence to D. Miklavčič, Faculty of Electrical Engineering, University of Ljubljana, Tržaška 25, SI-1000 Ljubljana, Slovenia. Electronic mail: damijan@svarun.fe.uni-lj.si

but the resulting error is difficult to estimate. And third, the uniform thickness of the membrane is a realistic condition that is very hard to meet in building a finite-elements model of an irregularly shaped cell.

In this paper, we describe an approach that reduces the difficulties mentioned above, allowing for determination of the ITV on irregularly shaped single cells, as well as cells in tissues. We describe a method for constructing realistic

models of irregularly shaped cells based on microscopic imaging. This provides a possibility to determine the ITV on the same cells on which an experiment was carried out, which can be of considerable importance in understanding and interpretation of the data. We also show how the finite-thickness, nonzero-conductivity membrane can be replaced by a boundary condition assigned to the interface between the cell interior (the cytoplasm) and the exterior.

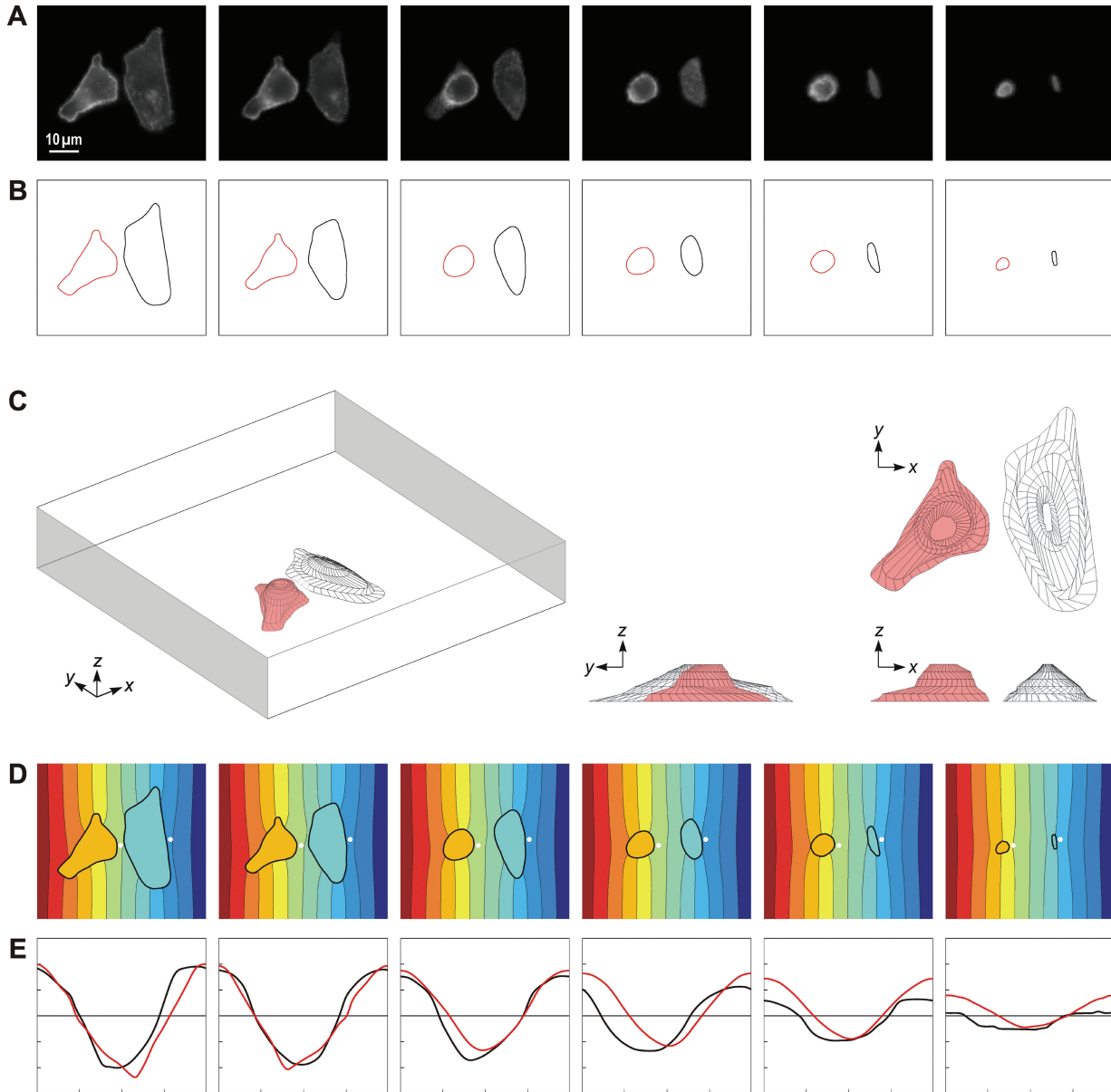


**FIGURE 1.** (A) Fluorescence images (8 bit) of two irregularly shaped CHO cells stained with di-8-ANEPPS. The images represent six cross-sections of the cells, acquired from the bottom to the top of the cells in  $1 \mu\text{m}$  steps. (B) The corresponding contours of the cell edges for a given cross-section. (C) The three-dimensional geometry of the cell models constructed from the cross-sections. The interior of the rectangular block represents the extracellular medium, the gray-shaded faces are the electrodes, and the other four faces are insulating. (D) The computed distribution of the electric potential for each of the six cross-sections. The black curves represent the equipotentials, and the white circles mark the start of the path along which the normalized arc length is measured counterclockwise. The contours separating the colors correspond, from left to right, to electric potential decrements of 50 mV. (E) The calculated ITV for the left (red) and the right cell (black). The plot ranges are identical to those shown in more detail in Figs. 5–7, with the horizontal ticks marking 0.25 increments of the relative arc length, and vertical ticks marking 50 mV increments of the ITV.

This efficiently eliminates the problems related to the modeling of a realistic cell membrane.

## METHODS

### *Construction of the Model*

The three-dimensional model of an irregularly shaped biological cell was constructed from a sequence of microscopic fluorescence images representing cross-sections of a Chinese hamster ovary (CHO) cell attached to the cover glass. The fluorescence images were obtained by staining the cell with fluorescent dye di-8-ANEPPS. The dye emits a strong fluorescence when it binds to the membrane, thereby making the cell edges visible. Besides, its fluorescence is linearly proportional to the voltage on the membrane, and can therefore be used for the measurements of the ITV (see later for details). The cross-sections were obtained by shifting the focus on a fluorescence microscope (Zeiss AxioVert 200, objective  $\times 100$ , oil immersion, Zeiss, Germany) in constant steps of  $1 \mu\text{m}$  from the bottom to the top of the cell Fig. 1a. The images were acquired using a cooled CCD camera (VisiCam 1280, Visitron, Germany) and MetaMorph 5.0 software (Visitron, Germany), and converted from grayscale (8 bit) to black and white (1 bit) in Corel PhotoPaint 11.0 (Corel Corp., Ottawa, Canada). Subsequent processing was performed on a PC equipped with a 2.8 GHz Pentium IV processor and 1 GB RAM. Using FEMLAB 3.1 package (COMSOL Inc., Burlington, MA) with MATLAB 6.5 (MathWorks Inc., Natick, MA, USA), the contours of the cell were detected using *flim 2 curve* (Fig. 1b), transformed to solid planes with 35 edges with *solid 2*, and the planes were connected into a 3D object using *loft* to obtain the model of the cell. This model was then imported to the FEMLAB workspace, where it was positioned at the bottom of a rectangular block, thereby mimicking the cell attached with its bottom to the cover glass (Fig. 1c). To construct a model of several cells, this procedure was repeated for each cell separately (in this paper we illustrate this for the case of two cells).

As discussed in the Introduction, direct incorporation of a realistic cell membrane (i.e. a very thin layer of very small, yet non-zero thickness surrounding the cell) into the model is technically very problematic. Unless the distribution of the electric field, current density, and/or electric potential *within the membrane* is of interest, this can be avoided. Namely, the effect of the membrane on these electric quantities in the cell interior and exterior is equivalent to the effect of a corresponding surface conductivity assigned to the interface between the interior and the exterior. More precisely, as the specific conductivity of the membrane—typically about  $5 \times 10^{-7} \text{ S/m}^8$ —is at least five orders of magnitude lower than the specific conductivities of the aqueous media surrounding it, the current flows through the membrane practically orthogonally to its surface. Consequently, in the membrane the total current density is vir-

tually equal to its normal component alone ( $J$ ), which is given by

$$J = \frac{\sigma_m(V_o - V_i)}{d}, \quad (1)$$

where  $\sigma_m$  is the specific membrane conductivity,  $d$  is the membrane thickness and  $V_o, V_i$  are the electric potentials at the outer and inner surface of the membrane, respectively. Here  $J, V_o$ , and  $V_i$  are functions varying with the position on the membrane, while  $\sigma_m$  and  $d$  are constants. For the purpose of determining the induced transmembrane voltage, the events inside the membrane layer are not relevant, and the ratio  $\sigma_m/d$  can be treated as a single entity—the specific surface conductivity,  $\kappa_m = \sigma_m/d$ . The interface between the cell interior (the cytoplasm) and the cell exterior is then characterized by

$$J = \kappa_m(V_o - V_i). \quad (2)$$

Despite the membrane as such being absent from the model, the drop of electric potential at such an interface is equivalent to the transmembrane voltage induced on a membrane with a specific conductivity  $\sigma_m$  and thickness  $d$ . In models constructed in this way, the mesh of finite elements is generated without difficulty, as very small (and possibly very irregularly shaped) elements corresponding to the membrane itself are avoided.

The computation of the functions  $J, V_o$ , and  $V_i$  was performed in FEMLAB by introducing two application modes, cell exterior (extracellular medium) being active in the first, and the cell interior (cytoplasm) in the second mode. Both application modes were of a static current density type. For models containing several cells, an additional application mode active in the cytoplasm of each cell was introduced, and the functions  $J_1, J_2, \dots$  and  $V_o, V_{i1}, V_{i2}, \dots$  were computed.

The specific conductivity of the cell interior was set to 0.2 S/m, a typical conductivity of the cell cytoplasm,<sup>14</sup> and the specific conductivity of the rest of the block (the cell exterior) was set to 0.15 S/m, which is a typical value of the low conductivity extracellular medium.<sup>34</sup> Two of the opposite vertical faces of the block were modeled as electrodes, which was done by assigning fixed electric potentials; 1 V to one electrode, and 0 V to the other (ground). The electrodes were positioned 0.01 cm apart to obtain the voltage-to-distance ratio of 100 V/cm. The remaining four faces of the block were modeled as insulating surfaces, the bottom one representing the cover glass. At the boundary surface between the cell interior and exterior, the normal component of the current density was set corresponding to Eq. (2) with a negative sign ( $-J$ ) in the mode corresponding to the cell exterior, and with a positive sign in the mode corresponding to the cytoplasm (or, with several cells, in all such modes). The specific surface conductivity was set at  $\kappa_m = 100 \text{ S/m}$ ,<sup>2</sup> which is the ratio between a specific

membrane conductivity of  $5 \times 10^{-7}$  S/m<sup>8</sup> and a membrane thickness of 5 nm.<sup>1</sup>

After the mesh was generated, the electric potential was computed using FEMLAB's stationary nonlinear *Conjugate gradients* solver with *Algebraic multigrid* preconditioner Fig. (1d). The induced transmembrane voltage (ITV) was calculated as the difference between electric potentials on the two sides of the boundary surface separating the inside and outside of the cell, i.e. as  $ITV = V_i - V_o$ . The ITV was then plotted as a function of relative arc length Fig. (1e).

#### Potentiometric Fluorescence Measurements

To experimentally determine the ITV on cells of irregular shape, we used di-8-ANEPPS, a fast potentiometric fluorescence dye which binds to the cell membrane, its fluorescence intensity varying linearly with the change in the ITV.<sup>2, 13, 15, 30</sup> The linear response of the dye was found for voltages ranging from  $-280$  mV to  $+140$  mV,<sup>4</sup> as well as from 0 to  $+250$  mV.<sup>26</sup>

CHO cells were grown on a cover glass in the culture medium (HAM-F12, Sigma-Aldrich, Steinheim, Germany). When cells attached to the glass (usually after 5–7 h), the culture medium was replaced with SMEM medium (Spinner's modification of the MEM, Gibco, USA) containing  $30 \mu\text{M}$  of di-8-ANEPPS and 0.05% of Pluronic (both Molecular Probes, Leiden, Netherlands). After staining for 12 min at  $4^\circ\text{C}$ , the cells were washed thoroughly with pure SMEM to remove the excess dye. Before the experiments, SMEM was replaced with an iso-osmotic buffer consisting of 10 mM potassium phosphate buffer (pH 7.4), 250 mM sucrose, and 1 mM  $\text{MgCl}_2$ . First, the cross-section fluorescence images of the cells were acquired (excitation 490 nm, emission 605 nm) as described in the previous section. Then, the same cells were exposed to a 40 V of voltage applied for a duration of 150 ms on two parallel electrodes with a 4 mm distance between them (voltage-to-distance ratio 100 V/cm). During the pulse, the fluorescence image of the lowermost level of the cell was acquired (excitation 490 nm, emission 605 nm). Five consecutive pulses of 150 ms duration were applied with a delay of 4 s and during each pulse the image was acquired. The control image, which was acquired before the train of pulses was delivered, was subtracted from these images and the corrected images were then averaged to increase the signal-to-noise ratio. The changes in the fluorescence of the dye in the membrane were quantified by measurements of gray levels of the region of interest, which was a line encircling the cell at the site of the membrane. Using a calibration curve obtained in a separate experiment (see below), the fluorescence changes were transformed to the values of the ITV, which were plotted on a graph as a function of the relative arc length. The images were acquired and processed

with the same imaging system as described in the previous section.

#### Calibration of the Fluorescent Dye

CHO cells were grown and stained with di-8-ANEPPS as described above. After washing, the SMEM was replaced with the calibrating medium consisting of 10 mM Hepes buffer (pH 7.5, Merck, Darmstadt, Germany), 140 mM NaCl/KCl and  $1 \mu\text{M}$  valinomycin (Sigma-Aldrich, Steinheim, Germany). The concentrations of NaCl and KCl were adjusted to obtain 3, 10, 50, and 140 mM concentrations of KCl, corresponding to membrane voltages of  $-99$ ,  $-68$ ,  $-27$ , and 0 mV, respectively. The voltages were obtained using the Nernst equation, assuming the intracellular  $\text{K}^+$  concentration of  $140 \text{ mM}$ <sup>1</sup> and considering that the membrane voltage corresponds to  $\text{K}^+$  equilibrium in the presence of valinomycin. After 4 min of incubation in the calibration medium with the lowest KCl concentration (3 mM), the image was acquired and the medium was replaced with the one with higher KCl concentration. This procedure was repeated until 140 mM concentration was reached. The average gray value of the whole line (region of interest) encircling the cell was determined for each image acquired. These values were then transformed to relative changes of the di-8-ANEPPS fluorescence and were plotted versus the voltage. The measurements were performed on three cells and the results are presented in the Fig. 2 as the mean  $\pm$  SD. Linear regression was performed on the measured values to obtain the calibration curve with a slope of 6%/100 mV. Despite the linear response of the dye, the error margins in the calibration curve suggest that the measured ITV values obtained from this curve can deviate considerably from the actual ITV. Also empirically, the ITV measurements with di-8-ANEPPS are characterized by extreme

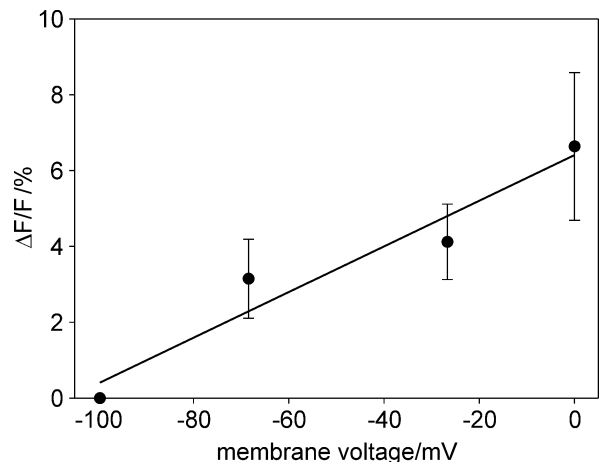


**FIGURE 2.** Calibration curve for di-8-ANEPPS. The measurements represent the mean of the relative changes in the fluorescence ( $\Delta F/F$ )  $\pm$  SD ( $n = 3$ ). The slope of the calibration curve (6%/100 mV) was determined from the linear regression curve.

sensitivity of the dye fluorescence to the environment<sup>30</sup> and intense noise-like spatial fluctuations (see e.g. Ref.<sup>24</sup>). To a certain extent, with a faster imaging system these errors can be reduced using ratiometric measurements,<sup>30</sup> but such a system was not available in our experiments. The images were acquired and processed with the same imaging system as described in the Construction of the Model section.

### NUMERICAL COMPUTATION OF THE ITV AND COMPARISON WITH OTHER METHODS

Reliability of a numerically determined ITV is in general open to doubt, as there are several steps in the modeling and subsequent computation where errors could potentially arise. The results obtained by the method introduced in Construction of the Model section were therefore verified by comparing it with the analytically derived ITV for a spherical cell and a tilted oblate spheroidal cell. In addition, the ITV computed for a model of two irregularly shaped CHO cells photographed under a microscope was compared with the ITV measured on these two cells by means of a potentiometric fluorescent dye, and also with the ITV computed for a simplified model of the same two cells each represented as a hemiellipsoid.

#### Validation by Comparison with two Analytical Solutions

##### A Spherical Cell

Under physiological conditions, the transmembrane voltage (ITV) induced by an electric field  $E$  on a spherical cell with outer radius  $R$  is given by Schwan's equation<sup>35</sup>

$$\text{ITV} = f_s E R \cos \varphi \quad (3)$$

where  $\varphi$  is the angle between the direction of the field and the line connecting the center of the cell to the point of interest and  $f_s$  is a function reflecting the electric and dimensional properties of the cell and the surrounding medium.<sup>21</sup>

$$f_s = \frac{3\lambda_o [3dR^2\lambda_i + (3d^2R - d^3)(\lambda_m - \lambda_i)]}{2R^3(\lambda_m + 2\lambda_o)(\lambda_m + \frac{1}{2}\lambda_i) - 2(R-d)^3(\lambda_o - \lambda_m)(\lambda_i - \lambda_m)} \quad (4)$$

In Eq. (4),  $\lambda_o$ ,  $\lambda_i$ , and  $\lambda_m$  are the specific conductivities of the extracellular medium, cytoplasm and the membrane, respectively, and  $d$  is the thickness of the membrane. Under physiological conditions, where  $\lambda_m$  is at least five orders of magnitude smaller than both  $\lambda_o$  and  $\lambda_i$ ,  $f_s$  is very close to the value of  $3/2$ , and the Schwan's equation is sometimes also written with  $f_s$  replaced by this explicit constant.

Schwan's equation provides a precise description of the ITV on a single spherical cell, and was as such used as the first test of the method of numerical determination of the ITV described in this paper. Figure 3b shows the ITV

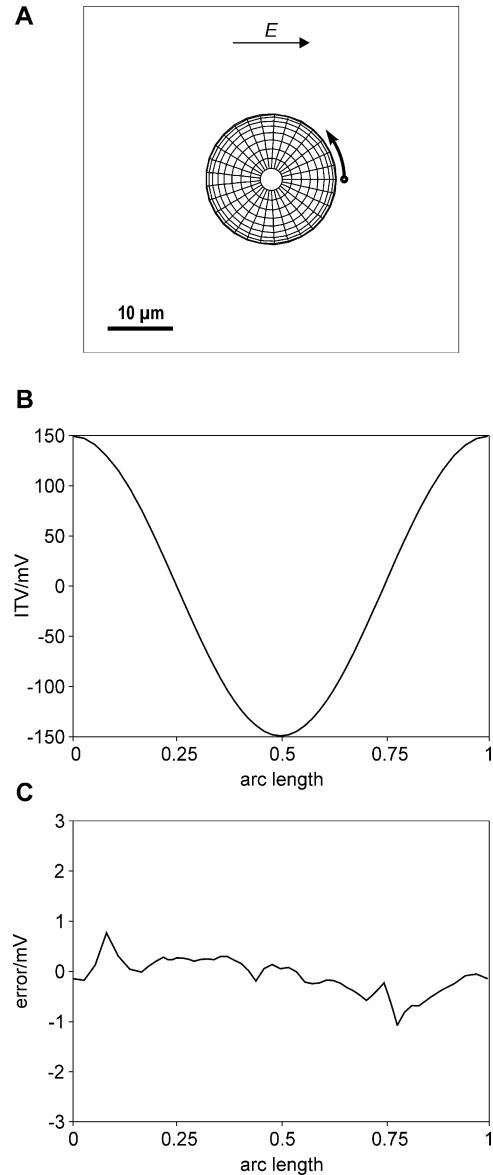


**FIGURE 3. (A) Geometry of a spherical cell. The arrow denotes the start and the direction of the path along which the normalized arc length is measured. (B) Computed ITV for a spherical cell with a membrane modeled as a boundary condition. (C) The difference between the computed and analytically derived ITV. The calculations were performed for a spherical cell with  $R = 10 \mu\text{m}$ ,  $\lambda_o = 1 \text{ S/m}$ ,  $\lambda_i = 0.2 \text{ S/m}$ ,  $\lambda_m = 5 \times 10^{-7} \text{ S/m}$ ,  $d = 5 \text{ nm}$ , and  $E = 100 \text{ V/cm}$ .**

computed using this method and Fig. 3c shows the error with respect to Schwan's equation (note that the y-scale is much smaller than in Fig. 3b). Both the analytical and the numerical solution were determined for a spherical cell with  $R = 10 \mu\text{m}$ ,  $\lambda_o = 1 \text{ S/m}$ ,  $\lambda_i = 0.2 \text{ S/m}$ ,  $\lambda_m = 5 \times 10^{-7} \text{ S/m}$ , and  $d = 5 \text{ nm}$ . The cell was exposed to an electric field of  $100 \text{ V/cm}$ , which was, in the numerical solution, generated by applying  $1 \text{ V}$  to a pair of rectangular parallel plate electrodes  $0.01 \text{ cm}$  apart. The cell was

centered between them, occupying a region in which the inhomogeneity of the field was everywhere below 1%.

The comparison with Schwan's equation shows that the error due to numerical computation varies with the position, but remains in the range between  $-1.07$  and  $0.77$  mV (less than 0.72% of the maximum value of the ITV, Fig. 3c), sufficiently accurate for any practical purpose. This error is mostly due to the finite size of the modeled electrodes and the space between them, and to some extent also due to nonzero size of the elements. This was verified by computing the ITV: (i) on the model of a spherical cell where the mesh was constructed from smaller finite elements (18,168 elements instead of 3746); (ii) on the same model of a spherical cell with electrodes larger (2.25 times the original surface) and further apart (1.5 times the original distance). In the first case (finer mesh), the maximum error between the computed and analytically derived ITV decreased from 0.72 to 0.46%, while in the second case (larger electrodes) the error decreased from 0.72% to 0.53%.

The main advantage of replacing the cell membrane with a boundary condition is that the mesh elements corresponding to the membrane are avoided. As described in the Introduction, if the membrane is instead modeled explicitly (i.e. built from mesh elements), its thickness must typically be exaggerated by an order of magnitude or more, otherwise the number of mesh elements is far too large to be handled by a computer. To compensate for this, the membrane can be assigned a correspondingly higher specific conductivity  $\lambda_m' = (d'/d) \times \lambda_m$ . Table 1 illustrates how the decrease of membrane thickness from exaggerated values towards realistic ones is accompanied by a rapid increase in the number of elements forming the mesh, and consequently also in the time needed for generating the mesh and solving the problem. With the PC and the FEMLAB software used in this study (see Construction of the Model section), the calculation of the solution was not possible for a membrane thinner than  $0.3 \mu\text{m}$ .

### An Oblate Spheroidal Cell

An example of a more complex geometry for which the analytical solution is still attainable is that of a spheroidal cell. The generalizations of Schwan's equation for these cases can be found in the literature.<sup>9,10,22,45</sup> Figure 4a shows an oblate spheroidal (disc-shaped) cell with its axis of rotational symmetry tilted by  $45^\circ$  with respect to the direction of the field. The ITV computed using our method is shown in Fig. 4b, and the error with respect to the analytical solution in Fig. 4c. The radii of the spheroidal cell were 2, 10, and  $10 \mu\text{m}$ , while the other parameters were the same as in the case of the spherical cell described in the preceding subsection. The error in the numerical computation ranged from  $-0.94$  mV to  $1.98$  mV, which is less than 2% of the maximum value of the ITV. Also in this case, the error was reduced further by using smaller finite elements (to 0.41% by using 69,772 elements instead of 9870). Thus, despite less symmetry in cell shape than in the case of a spherical cell, and despite the lack of symmetry in the position of the cell with respect to the field, the method again yields results with sufficient accuracy for any practical purpose.

### Comparison with Fluorescence Measurements

The model of two irregularly shaped cells was constructed from six cross-sections of the cells photographed under a microscope, as described in detail in the Methods section (Figs. 1a–c). The electric potential was computed on the finite-elements rendering of this model, as shown in Fig. 1d, and the ITV for each cell was then calculated as the difference between the electric potentials in the cell interior and exterior. Figure 1e shows the computed ITV for each of the six cross-sections (counted from the bottom of the cells) for the left cell (red curve) and the right cell (black curve), respectively. Towards the top of the cells the cross-sections become smaller, and so does their effect on the external field. As a consequence, the amplitudes of the ITV gradually decrease, and in the topmost cross-section

**TABLE 1. The influence of the membrane thickness on the number of mesh elements, the time required for mesh generation, and the time required for solution (i.e., determination of the electric potential) for a spherical cell.**

Numerical model	No. of mesh elements	Time for mesh	Time for solution
Membrane modeled implicitly through the boundary condition			
$d = 5 \text{ nm}$ , $\lambda_m = 5 \times 10^{-7} \text{ S/m}$	3746	< 1 s	2,6 s
Membrane modeled explicitly			
$d' = 1.5 \mu\text{m}$ , $\lambda_m' = 1.5 \times 10^{-4} \text{ S/m}$	9738	< 1 s	7 s
$d' = 1 \mu\text{m}$ , $\lambda_m' = 1 \times 10^{-4} \text{ S/m}$	18376	2 s	13 s
$d' = 0.5 \mu\text{m}$ , $\lambda_m' = 0.5 \times 10^{-4} \text{ S/m}$	73305	15 s	60 s
$d' = 0.3 \mu\text{m}$ , $\lambda_m' = 0.3 \times 10^{-4} \text{ S/m}$	198895	45 s	179 s
$d' = 0.2 \mu\text{m}$ , $\lambda_m' = 0.2 \times 10^{-4} \text{ S/m}$	410502	400 s	Out of memory

*Note.*  $d$  and  $\lambda_m$  are the thickness and the conductivity of the implicitly modeled membrane, respectively, which are incorporated in the boundary condition of surface conductivity, while  $d'$  is the thickness of the explicitly modeled membrane, for which the conductivity is chosen as  $\lambda_m' = (d'/d) \times \lambda_m$

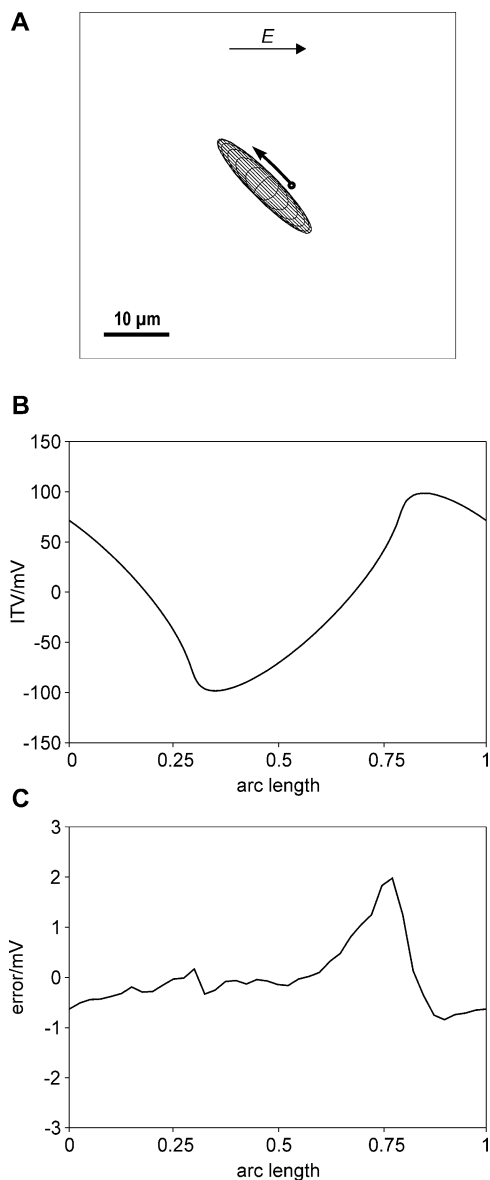


**FIGURE 4.** (A) Geometry of an oblate spheroidal cell. The arrow denotes the start and the direction of the path along which the normalized arc length is measured. (B) Computed ITV for this cell with a membrane modeled as a boundary condition. (C) The difference between the computed and analytically derived ITV. The calculations were performed for a cell with radii of 10, 10, and 2 μm, and the other parameters are as in Fig. 3.

they are only 30 and 18% of the amplitudes at the bottom level of the left and the right cell, respectively (Fig. 1e).

The computed values of the ITV for the left and the right cell at the level of the lowermost surface were than compared to the experimentally measured ITV for the same two cells, by using di-8-ANEPPS. The dye binds to the membrane, and within the linear range a 6% change in fluorescence intensity corresponds to approximately 100 mV change in transmembrane voltage (Fig. 2). The results presented in Figs. 5b and 5c show that for each

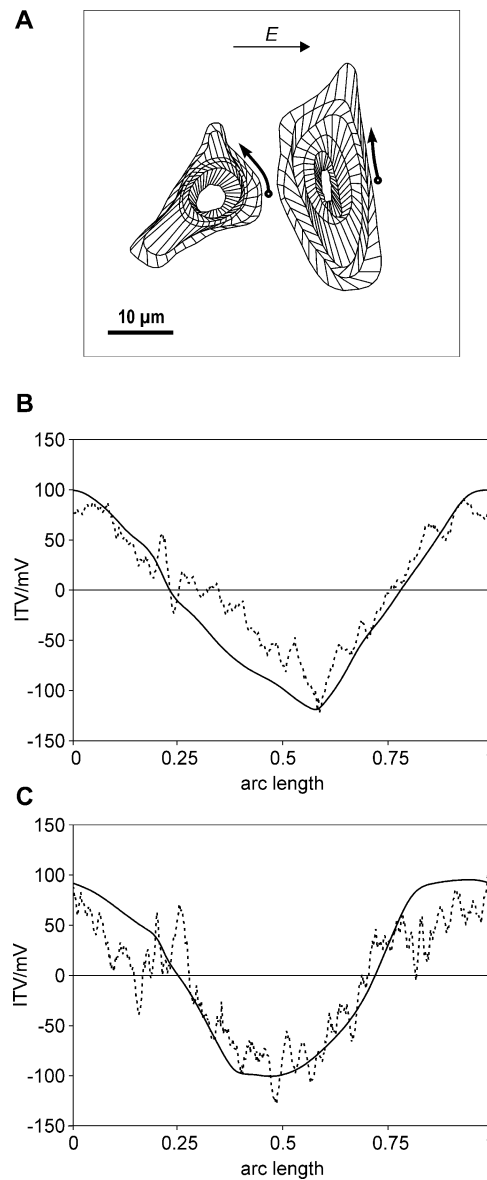


**FIGURE 5.** (A) Geometry of the two irregularly shaped cells (see also Fig. 1). The arrow denotes the start and the direction of the path along which the normalized arc length is measured. (B) Comparison of the ITV determined numerically (solid) and experimentally (dashed) for the lowermost cross-section of the cell on the left. (C) Same as in B, but for the cell on the right. The measured ITV was obtained by staining CHO cells with di-8-ANEPPS (excitation 490 nm, emission 605 nm), and exposing them for 100 ms to 40 V applied to a pair of flat parallel stainless-steel electrodes 4 mm apart.

cell, the experimental ITV curve (dashed) is similar in large-scale shape and amplitude to the corresponding computed ITV curve (solid).

#### *Comparison with Simplified Cell Shapes*

To evaluate how a simplification of the geometry affects the computed ITV, the irregularly shaped cells treated in

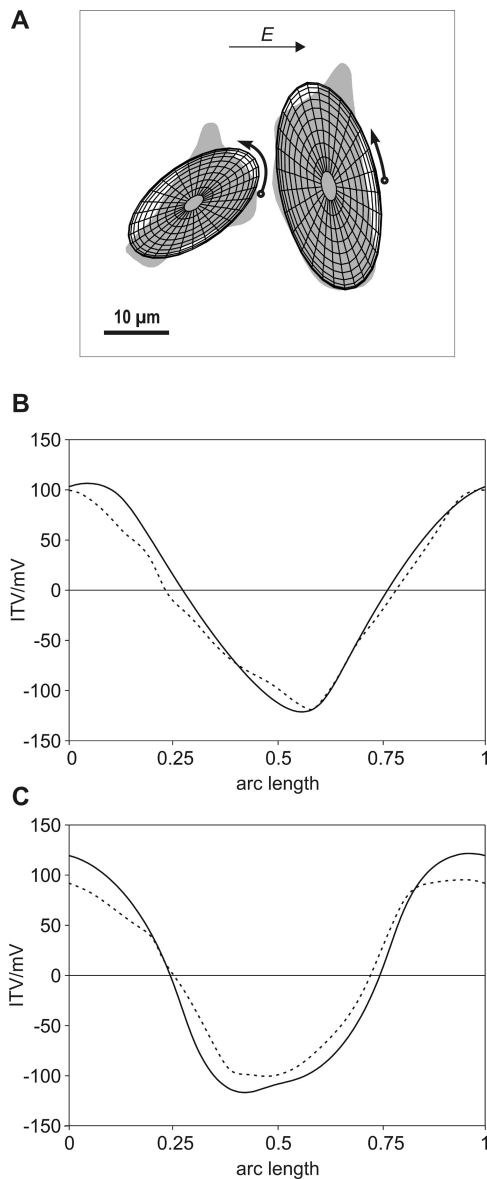


**FIGURE 6.** Comparison of the model of two irregularly shaped cells from Fig. 5 with a simpler model of the same two cells represented by hemiellipsoids. (A) The geometry and the position of the hemiellipsoids with respect to the realistic model. The left hemiellipsoid had horizontal semi-axes  $11.5 \mu\text{m}$  and  $6 \mu\text{m}$ , the right one  $16$  and  $7.5 \mu\text{m}$ , and vertical semi-axes of both were  $6 \mu\text{m}$ . The arrows represent the start and the direction of the path along which the normalized arc length is measured. (B) The comparison of the ITV determined on the hemiellipsoid (solid line) with the more realistic model (dashed line) for the cell on the left. (C) Same as in B, but for the cell on the right. The computed ITV curves are for the lowermost cross-section.

Comparison with Fluorescence Measurement section were replaced by hemiellipsoids of the same height, with the other two dimensions and the position adjusted to resemble those of the original irregularly shaped cells (Fig. 6a). The membrane was again included as a boundary condition, and the electrical parameters were as in preceding subsec-

tions. The computed ITV for the lowermost level of the hemiellipsoids is shown with solid curves in Figs. 6b and 6c for the hemiellipsoid on the left and the hemiellipsoid on the right, respectively. The dashed curves give the ITV on the corresponding irregularly shaped cells. These results show that the differences in the ITV computed with simplified geometry when compared to the more realistic geometry are considerable. More precisely, the largest differences with respect to the maximum ITV are approximately 25 and 30% for the cell on the left and the cell on the right, respectively, and the average differences are approximately 10 and 17%, respectively. These deviations, although considerable, are still smaller than the noise inherent to experimental measurements of ITV such as those shown in Fig. 5.

## DISCUSSION

The distribution of the voltage induced on the cell membrane (the ITV) can be of interest in many theoretical and experimental settings, such as activation of voltage-dependent membrane channels and cell membrane electroporation. With cells of simple geometrical shapes, this distribution can be determined analytically<sup>9, 10, 21–23, 35</sup> but with irregularly shaped cells this can only be achieved experimentally<sup>2, 13, 15, 20, 25, 30</sup> or numerically<sup>5, 6, 12, 28, 32, 38, 39, 45</sup>. Frequently biological cells are modeled as simple geometrical objects (spheres, spheroids. . .) and, for more complicated cell shapes, by combining several such objects (e.g. hemispheres, circular or elliptic cylinders, etc.).<sup>3, 5, 6, 19, 22, 32, 45</sup> These models can be realistic for cells in suspensions, but cells growing in a dish or in tissues have markedly irregular shapes, and combinations of several simple geometrical objects are only rough approximations of their real shapes. In this paper we presented a method for construction of more realistic models of such cells from their cross-section images. In our case, each cell model was composed of six cross-sections transformed to solid planes with 35 edges, which is sufficient for a reasonably faithful representation of the real cell. In FEMLAB 3.1, all the planes from which the solid object is generated must have the same number of edges, and the object always has a flat top. Increasing the number of planes or the number of edges yields a more detailed model, but if carried out too far, this eventually results in difficulties in mesh generation. Because we were not using the confocal microscope, our images contained a considerable amount of the out-of-focus fluorescence, so performing the transformation of these images to 1-bit (black and white) images occasionally required manual correction of one or several edges of the cell.

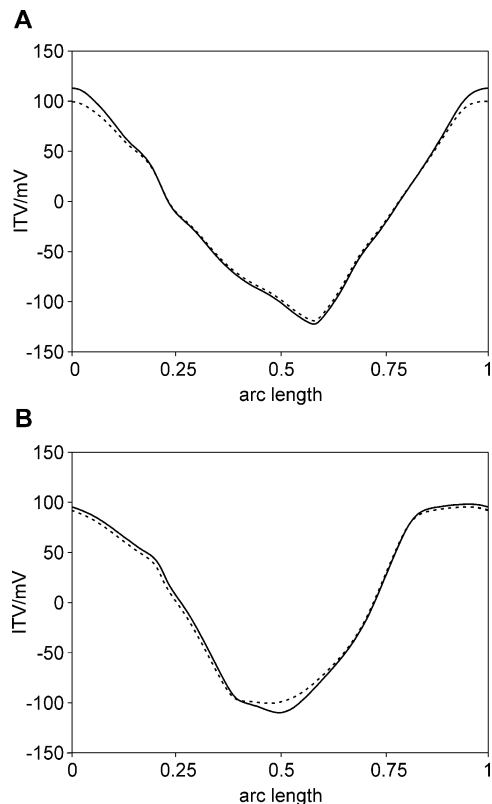
The ITV is the difference between the potentials on both sides of the membrane. Therefore in computing the ITV, the model of the cell cannot be a homogeneous solid with a low conductivity (which would suffice for determination of the external potential distribution, for example), but must have a conductive interior corresponding to the cytoplasm. As

Table 1 shows, it is practically impossible to incorporate a cell membrane of a realistic thickness into a finite-elements model of the cell. Furthermore, even if this thickness is exaggerated, it is problematic to make it uniform, particularly at the protrusions and edges of the cell, and pronounced nonuniformities can affect the calculation of the ITV considerably.<sup>22</sup> The method we present in this paper resolves these difficulties by replacing the membrane with a specific surface conductivity assigned to the interface between the cell interior and the exterior, whereby the conditions corresponding to the uniform thickness are automatically met. An additional advantage is that the model in which the explicit membrane is replaced by a boundary condition consists of a considerably lower number of mesh elements, and the solution is also obtained faster. To validate this method, the ITV computed using this method was compared with the analytical expression describing the ITV for the same cell (a sphere or a tilted spheroid), showing a very good agreement between both solutions (Figs. 3b and 3c, 4b and 4c).

The construction of a 3D model from the cross-section images and the replacement of an explicit membrane with a boundary condition were used to build a model of two irregularly shaped cells and to calculate the ITV on them. Because the model was built from the cross-sections of the same cells on which the experimental measurements of the ITV were performed, it was possible to compare the computed and the experimental results. As the errors of the presented method with respect to the analytical solution for a spherical and a tilted oblate spheroidal cell are very small (Figs. 3c and 4c), this can be considered as evidence that this method is a reliable and accurate one.

We found some discrepancies in the amplitudes of the computed and experimentally obtained ITV, mostly attributable to the calibration which was not performed on the same cells on which the experiment was carried. The obtained calibration slope of  $\sim 6\%$  was also lower than the slope obtained by other authors ( $\sim 9\%/100$  mV),<sup>13,30</sup> perhaps due to our selection of excitation and emission filters that were probably not perfect for the best response fluorescence with the chosen dye. To perform an experimental determination of the ITV at levels other than the lowermost one, one would have to use a confocal microscope, as on other microscopes higher levels contain the out-of-focus fluorescence from the regions above and below the observed one, which affects the measurements of the fluorescence. In contrast, the ITV can easily be investigated at any level using numerical methods including the one described in this paper.

Finally, in Comparison with Simplified Cell Shapes section we compared the ITV calculated on our detailed model and on a simplified model composed of two semiellipsoids. This comparison demonstrates that for cell shapes deviating significantly from a regular geometric object, computation of the ITV on the latter object can lead to deviations ranging into tens of percents (Fig. 6). Thus for cells with a com-



**FIGURE 7.** The effect of the mutual electrical screening of the cells on the ITV. (A) The ITV for the left cell in Fig. 5 with the right cell absent (solid line) and with the right cell present (dashed line). (B) The ITV for the right cell with the left cell absent (solid line) and with the left cell present (dashed line).

plicated shape, such as neurons, computations on the more realistic model can provide a better understanding of the response of the cells to an electric field. The construction of a model of such cells along the lines described in this paper is rather simple, and is probably worth the effort. In contrast, for cells having a simple shape, such as bacilli (approximated by prolate spheroids) or erythrocytes (oblate spheroids), computation of the ITV on a regular geometric object would suffice. In addition, if the only purpose of computing the ITV is to compare it to potentiometric experimental data that contain oscillations similar to those shown in Fig. 5, the ITV computed with either a simplified or a more realistic geometry will likely be within these oscillations, showing a similar degree of agreement.

The results presented above demonstrate that the computational approach to ITV determination is a useful technique either by itself or as a complement to experimental studies. Moreover, it can provide insights that would be rather difficult to obtain in the actual experimental environment. As an example, Figs. 7a and 7b show, in solid curves, the computed ITV for the left and the right cell from Fig. 5, respectively, but this time with the other cell absent; for comparison, the dashed curves give the computed ITV

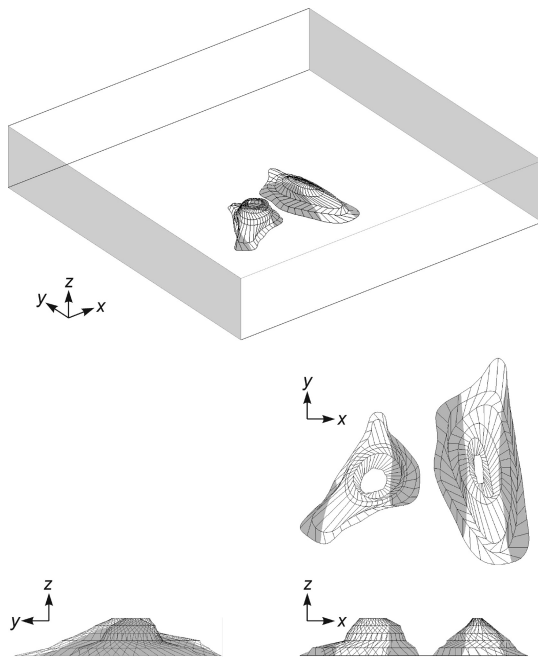


**FIGURE 8.** The permeabilized regions of the cell membrane. A voltage of 3 V was applied to the electrodes of the same model of two irregular cells as shown in Figs. 1 and 5. The permeabilized parts of the membrane are colored gray and represent the regions where the ITV exceeds 250 mV.

when both cells are present. In a finite-elements model, this is an elementary modification of the earlier analysis, as the object corresponding to one of the cells is simply removed from the rectangular block representing the extracellular medium. In the case shown here, the differences are not large, but they are detectable, reflecting the mutual electrical shielding of one cell by the other. This is an illustration of the often-neglected fact that even when not in direct physical contact, the neighboring cells affect the ITV of each other (for a detailed treatment of the case of spherical cells, see e.g. Refs.<sup>32,39</sup>).

Another example of a potentially useful application of the described method is the investigation of cell membrane electropermeabilization. As mentioned in the Introduction, this phenomenon occurs in those regions of the cell membrane where the ITV exceeds a certain threshold value, typically ranging from 250 to 1000 mV.<sup>42,44</sup> The regions permeabilized by an exposure to electric pulses of given amplitude can easily be determined with our method, by marking in the model the areas where the ITV is above the chosen threshold value. In Fig. 8, a voltage of 3 V is applied to the electrodes of the same model of two irregular cells treated in the preceding sections of the paper, and assuming the threshold ITV of 250 mV, the permeabilized membrane regions are shown in gray. The same approach is applicable in investigating the location of the open and closed voltage-gated membrane channels. Since the presented model treats the membrane as electrically passive (i.e., having

a constant electric conductivity), it cannot predict the ITV modification caused by opening or closing of voltage-gated channels or forming of electropores, since these events alter the conductivity of the membrane.<sup>1</sup>

The computations presented in the paper are based on the conditions occurring in an exposure to a time-constant (DC) field. Since the charging time of the membrane is in the order of microseconds, the method is also applicable for computing the ITV induced at any given moment by fields that vary sufficiently slowly, e.g. alternating (AC) fields below 100 kHz. It cannot, however, be used for computation of the transients.

Finally, the presented methods of model construction from cross-section images and replacement of the membrane by a boundary condition can also be used to study more complicated cell geometries, such as several cells in contact, which represent a simple model of a tissue.

## ACKNOWLEDGMENTS

This work was supported by the Ministry of Higher Education, Science and Technology of the Republic of Slovenia. The authors wish to thank Dr Marko Puc for building the switcher device for delivery of electric pulses in the experiments.

## REFERENCES

- <sup>1</sup>Alberts, B., D. Bray, J. Lewis, M. Raff, K. Roberts, and J. D. Watson. *Molecular Biology of the Cell*, 3rd edn., New York: Garland, 1994.
- <sup>2</sup>Bedlack, R. S., M. Wei, S. H. Fox, E. Gross, and L. M. Loew. Distinct electric potentials in soma and neurite membranes. *Neuron* 13:1187–1193, 1994.
- <sup>3</sup>Buitenweg, J. R., W. L. Rutten, and E. Marani. Geometry-based finite-element modeling of the electrical contact between a cultured neuron and a microelectrode. *IEEE Trans. Biomed. Eng.* 50:501–509, 2003.
- <sup>4</sup>Cheng, D. K. L., L. Tung, and E. A. Sobie. Nonuniform responses of transmembrane potential during electric field stimulation of single cardiac cells. *Am. J. Physiol.* 277:H351–H362, 1999.
- <sup>5</sup>Fear, E. C., and M. A. Stuchly. Biological cells with gap junctions in low-frequency electric fields. *IEEE Trans. Biomed. Eng.* 45:856–866, 1998.
- <sup>6</sup>Fear, E. C., and M. A. Stuchly. Modeling assemblies of biological cells exposed to electric fields. *IEEE Trans. Biomed. Eng.* 45:1259–1271, 1998.
- <sup>7</sup>Gabriel, B., and J. Teissié. Fluorescence imaging in the millisecond time range of membrane electropermeabilization of single cell using a rapid ultra-low-light intensifying detection system. *Eur. Biophys. J.* 27:291–298, 1998.

<sup>1</sup> This could be addressed by sequentially modifying the electric properties of the membrane and recomputing the potential distribution. An example of such modification for a tissue exposed to an electric field can be found in Ref.<sup>41</sup>

- <sup>8</sup>Gascoyne, P. R. C., R. Pethig, J. P. H. Burt, and F. F. Becker. Membrane changes accompanying the induced differentiation of Friend murine erythroleukemia cells studied by dielectrophoresis. *Biochim. Biophys. Acta.* 1146:119–126, 1993.
- <sup>9</sup>Gimsa, J., and D. Wachner. Analytical description of the transmembrane voltage induced on arbitrarily oriented ellipsoidal and cylindrical cells. *Biophys. J.* 81:1888–1896, 2001.
- <sup>10</sup>Gimsa, J., and D. Wachner. On the analytical description of transmembrane voltage induced on spheroidal cells with zero membrane conductance. *Eur. Biophys. J.* 30:463–466, 2001.
- <sup>11</sup>Golzio, M., L. Mazzolini, P. Moller, M. P. Rols, and J. Teissie. Inhibition of gene expression in mice muscle by in vivo electrically mediated siRNA delivery. *Gene Therapy* 12:246–251, 2005.
- <sup>12</sup>Gowrishankar, T. R., and J. C. Weaver. An approach to electrical modeling of single and multiple cells. *Proc. Natl. Acad. Sci. U.S.A.* 100:3203–3208, 2003.
- <sup>13</sup>Gross, D., L. M. Loew, and W. Webb. Optical imaging of cell membrane potential changes induced by applied electric fields. *Biophys. J.* 50:339–348, 1986.
- <sup>14</sup>Harris, C. M., and D. B. Kell. The radio-frequency dielectric properties of yeast cells measured with a rapid, automated, frequency-domain dielectric spectrometer. *Bioelectrochem. Bioenerg.* 11:15–28, 1983.
- <sup>15</sup>Hassan, N., I. Chatterjee, N. G. Publicover, and G. L. Craviso. Mapping membrane-potential perturbations of chromaffin cells exposed to electric fields. *IEEE Trans. Plasma Sci.* 30:1516–1524, 2002.
- <sup>16</sup>Heller, R., R. Gilbert, and M. J. Jaroszeski. Clinical applications of electrochemotherapy. *Adv. Drug. Deliv. Rev.* 35:119–129, 1999.
- <sup>17</sup>Hibino, M., H. Itoh, and K. Kinoshita. Time courses of cell electroporation as revealed by submicrosecond imaging of transmembrane potential. *Biophys. J.* 64:1789–1800, 1993.
- <sup>18</sup>Hibino, M., M. Shigemori, H. Itoh, K. Nagayama, and K. Kinoshita. Membrane conductance of an electroporated cell analyzed by submicrosecond imaging of transmembrane potential. *Biophys. J.* 59:209–220, 1991.
- <sup>19</sup>Huang, X., D. Nguyen, D. W. Greve, and M. M. Domach. Simulation of microelectrode impedance changes due to cell growth. *IEEE Sensors J.* 4:576–583, 2004.
- <sup>20</sup>Knisley, S. B., T. F. Blitchington, B. C. Hill, A. O. Grant, W. M. Smith, T. C. Pilkington, and R. E. Ideker. Optical measurements of transmembrane potential changes during electric field stimulation of ventricular cells. *Circ. Res.* 72:255–268, 1993.
- <sup>21</sup>Kotnik, T., F. Bobanovič, and D. Miklavčič. Sensitivity of transmembrane voltage induced by applied electric fields – a theoretical analysis. *Bioelectrochem. Bioenerg.* 43:285–291, 1997.
- <sup>22</sup>Kotnik, T., and D. Miklavčič. Analytical description of transmembrane voltage induced by electric fields on spheroidal cells. *Biophys. J.* 79:670–679, 2000.
- <sup>23</sup>Kotnik, T., and D. Miklavčič. Second-order model of membrane electric field induced by alternating external electric fields. *IEEE Trans. Biomed. Eng.* 47:1074–1081, 2000.
- <sup>24</sup>Lee, D. C., and W. M. Grill. Polarization of a spherical cell in a nonuniform extracellular electric field. *Anal. Biomed. Eng.* 33:603–615, 2005.
- <sup>25</sup>Loew, L. M. Voltage sensitive dyes: Measurement of membrane potentials induced by DC and AC electric fields. *Bioelectromagnetics Suppl.* 1:179–189, 1992.
- <sup>26</sup>Lojewska, Z., D. L. Franks, B. Ehrenberg, and L. M. Loew. Analysis of the effect of medium and membrane conductance on the amplitude and kinetics of membrane potentials induced by externally applied electric fields. *Biophys. J.* 56:121–128, 1989.
- <sup>27</sup>Miklavčič, D., G. Pucihar, M. Pavlovec, S. Ribarič, M. Mali, A. Maček-Lebar, M. Petkovšek, J. Nastran, S. Kranjc, M. Čemažar, and G. Serša. The effect of high frequency electric pulses on muscle contractions and antitumor efficiency in vivo for a potential use in clinical electrochemotherapy. *Bioelectrochemistry* 65:121–128, 2005.
- <sup>28</sup>Miller, C. E., and C. S. Henriquez. Three-dimensional finite element solution for biopotentials: Erythrocyte in an applied field. *IEEE Trans. Biomed. Eng.* 35:712–718, 1988.
- <sup>29</sup>Mir, L. M., and S. Orlowski. Mechanisms of electrochemotherapy. *Adv. Drug Deliv. Rev.* 35:107–118, 1999.
- <sup>30</sup>Montana, V., D. L. Farkas, and L. M. Loew. Dual-wavelength ratiometric fluorescence measurements of membrane-potential. *Biochemistry* 28:4536–4539, 1989.
- <sup>31</sup>Neumann, E., S. Kakorin, and K. Toensing. Fundamentals of electroporative delivery of drugs and genes. *Bioelectrochem. Bioenerg.* 48:3–16, 1999.
- <sup>32</sup>Pavlin, M., N. Pavšelj, and D. Miklavčič. Dependence of induced transmembrane potential on cell density, arrangement, and cell position inside a cell system. *IEEE Trans. Biomed. Eng.* 49:605–612, 2002.
- <sup>33</sup>Pucihar, G., T. Kotnik, M. Kandušer, and D. Miklavčič. The influence of medium conductivity on electroporation and survival of cells in vitro. *Bioelectrochemistry* 54:107–115, 2001.
- <sup>34</sup>Rols, M. P., C. Delteil, M. Golzio, and J. Teissie. Control by ATP and ADP of voltage-induced mammalian-cell-membrane permeabilization, gene transfer and resulting expression. *Eur. J. Biochem.* 254:382–388, 1998.
- <sup>35</sup>Schwan, H. P. Electrical properties of tissue and cell suspensions. *Adv. Biol. Med. Phys.* 5:147–209, 1957.
- <sup>36</sup>Serša, G., M. Čemažar, and Z. Rudolf. Electrochemotherapy: advantages and drawbacks in treatment of cancer patients. *Cancer Ther.* 1:133–142, 2003.
- <sup>37</sup>Somiari, S., J. G. Malone, J. J. Drabick, R. A. Gilbert, R. Heller, M. J. Jaroszeski, and R. W. Malone. Theory and in vivo application of electroporative gene delivery. *Mol. Ther.* 2:178–187, 2000.
- <sup>38</sup>Stewart, D. A., T. R. Gowrishankar, and J. C. Weaver. Transport lattice approach to describing cell electroporation: use of a local asymptotic model. *IEEE Trans. Plasma Sci.* 32:1696–1708, 2004.
- <sup>39</sup>Susil, R., D. Šemrov, and D. Miklavčič. Electric field induced transmembrane potential depends on cell density and organization. *Electro. Magnetobiol.* 17:391–399, 1998.
- <sup>40</sup>Šatkauskas, S., M. F. Bureau, M. Puc, A. Mahfoudi, D. Scherman, D. Miklavčič, and L. M. Mir. Mechanisms of in vivo DNA electrotransfer: respective contributions of cell electroporation and DNA electrophoresis. *Mol. Ther.* 5:133–140, 2002.
- <sup>41</sup>Šel, D., D. Cukjati, D. Batiuskaite, T. Slivnik, L. M. Mir, and D. Miklavčič. Sequential finite element model of tissue electroporation. *IEEE Trans. Biomed. Eng.* 52:816–827, 2005.
- <sup>42</sup>Teissie, J., and M. P. Rols. An experimental evaluation of the critical potential difference inducing cell membrane electroporation. *Biophys. J.* 65:409–413, 1993.
- <sup>43</sup>Teissie, J., N. Eynard, B. Gabriel, and M. P. Rols. Electroporation of cell membranes. *Adv. Drug Deliver Rev.* 35:3–19, 1999.
- <sup>44</sup>Tsong, T. Y. Electroporation of cell membranes. *Biophys. J.* 60:297–306, 1991.
- <sup>45</sup>Valič, B., M. Golzio, M. Pavlin, A. Schatz, C. Faurie, B. Gabriel, J. Teissie, M. P. Rols, and D. Miklavčič. Effect of electric field induced transmembrane potential on spheroidal cells: theory and experiment. *Eur. Biophys. J.* 32:519–528, 2003.